

Minerva Access is the Institutional Repository of The University of Melbourne

Author/s:

Alquethamy, S;Ganio, K;Luo, Z;Hossain, SI;Hayes, AJ;Ve, T;Davies, MR;Deplazes, E;Kobe, B;McDevitt, CA

Title:

Structural and biochemical characterization of *Acinetobacter baumannii* ZnuA

Date:

2022-06-01

Citation:

Alquethamy, S., Ganio, K., Luo, Z., Hossain, S. I., Hayes, A. J., Ve, T., Davies, M. R., Deplazes, E., Kobe, B. & McDevitt, C. A. (2022). Structural and biochemical characterization of *Acinetobacter baumannii* ZnuA. *Journal of Inorganic Biochemistry*, 231, <https://doi.org/10.1016/j.jinorgbio.2022.111787>.

Persistent Link:

<https://hdl.handle.net/11343/300002>

# 1     **Structural and biochemical characterization of *Acinetobacter baumannii* ZnuA**

2     Saleh Alquethamy<sup>1</sup>, Katherine Ganio<sup>1</sup>, Zhenyao Luo<sup>2,3,4</sup>, Sheik Imamul Hossain<sup>5</sup>, Andrew J. Hayes<sup>1</sup>,  
3     Thomas Ve<sup>2,3,4,6</sup>, Mark R. Davies<sup>1</sup>, Evelyne Deplazes<sup>2,5</sup>, Boštjan Kobe<sup>2,3,4,†</sup>, Christopher A.  
4     McDevitt<sup>1,†</sup>

5  
6     1. Department of Microbiology and Immunology, The Peter Doherty Institute for Infection and  
7     Immunity, The University of Melbourne, Melbourne, Victoria, Australia.

8     2. School of Chemistry and Molecular Biosciences, The University of Queensland, Brisbane,  
9     Queensland, Australia.

10    3. Australian Infectious Diseases Research Centre, The University of Queensland, Brisbane,  
11    Queensland, Australia.

12    4. Institute for Molecular Bioscience, The University of Queensland, Brisbane, Queensland,  
13    Australia.

14    5. School of Life Sciences, University of Technology Sydney, Ultimo, New South Wales, Australia.

15    6. Present Address: Institute for Glycomics, Griffith University, Queensland, Australia.

16

17    † Correspondence address: Boštjan Kobe, School of Chemistry and Molecular Biosciences, The  
18    University of Queensland, Brisbane, Queensland, Australia. Phone: +61-7-3365-2132. E-mail:

19    [b.kobe@uq.edu.au](mailto:b.kobe@uq.edu.au); Christopher A. McDevitt, Department of Microbiology and Immunology, The  
20    Peter Doherty Institute for Infection and Immunity, The University of Melbourne, Melbourne,  
21    Victoria, 3000, Australia. Phone: 61-3-8344-7200. E-mail: [christopher.mcdevitt@unimelb.edu.au](mailto:christopher.mcdevitt@unimelb.edu.au);

22

23    **Keywords:** *Acinetobacter baumannii*, zinc, solute-binding protein, ABC transporter, ZnuA, zinc  
24    homeostasis

25    **Running title:** Characterization of *A. baumannii* ZnuA

26

27 **ABSTRACT**

28 *Acinetobacter baumannii* is a Gram-negative nosocomial pathogen associated with significant  
29 disease. Crucial to the survival and pathogenesis of *A. baumannii* is the ability to acquire essential  
30 micronutrients such as Zn(II). Recruitment of Zn(II) by *A. baumannii* is mediated, at least in part, by  
31 the periplasmic solute-binding protein ZnuA and the ATP-binding cassette transporter ZnuBC. Here,  
32 we combined genomic, biochemical, and structural approaches to characterize *A. baumannii*  
33 AB5075\_UW ZnuA. Bioinformatic analyses using a diverse collection of *A. baumannii* genomes  
34 determined that ZnuA is highly conserved, with the binding site comprised by three strictly conserved  
35 histidine residues. The structure of metal-free ZnuA was determined at 2.1 Å resolution, with  
36 molecular dynamics revealing that loop  $\alpha 2\beta 2$ , which harbors the putative Zn(II)-coordinating residue  
37 His41, was highly mobile in the metal-free state. The contribution of the putative binding site histidine  
38 residues to Zn(II) binding was further probed by mutagenesis. Analysis of ZnuA mutant variants was  
39 performed by quantitative metal binding assays, differential scanning fluorimetry and affinity  
40 measurements, which showed that all three histidine residues contributed to Zn(II)-recruitment, albeit  
41 to different extents. Collectively, these analyses provide insight into the mechanism of Zn(II)-binding  
42 by *A. baumannii* ZnuA and expand our understanding of the functional diversity of Zn(II)-recruiting  
43 proteins.

44

45 **1. INTRODUCTION**

46 The *d*-block metal ion zinc [Zn(II)] is the second most abundant transition metal ion in humans and  
47 is crucial for all life forms. Zinc is predicted to interact with approximately 6% of the proteome of  
48 prokaryotes, wherein the metal ion serves in structural and catalytic roles [1-3]. The essentiality of  
49 Zn(II) necessitates that pathogenic microorganisms use efficacious recruitment mechanisms to  
50 acquire the metal ion from the host environment. Accordingly, vertebrate hosts employ a variety of  
51 withholding mechanisms to restrict the bioavailability of nutrient metal ions such as Zn(II). To  
52 overcome Zn(II) withholding at the host-pathogen interface, bacteria such as *Acinetobacter*  
53 *baumannii* [4], *Pseudomonas aeruginosa* [5, 6], *Escherichia coli* [7], *Salmonella enterica* serovar  
54 Typhimurium [8], and *Streptococcus pneumoniae* [9-11] can employ a variety of high affinity Zn(II)  
55 scavenging mechanisms.

56 *A. baumannii* is an opportunistic human pathogen found predominantly in hospitals and aged-  
57 care facilities. The emergence of multidrug-resistant *A. baumannii* isolates has prompted the World  
58 Health Organization (WHO) and the Centers for Disease Control and Prevention (CDC) to classify  
59 *A. baumannii* as a serious threat to human health [12]. Acquisition of Zn(II) is essential for *A.*  
60 *baumannii* pathogenesis and survival, and its uptake is mediated by the ATP-binding cassette (ABC)  
61 transporter, ZnuBC, and the periplasmic solute-binding protein (SBP), ZnuA [4, 13]. Disruption of  
62 any component of the *A. baumannii* ZnuABC permease has been shown to result in a pronounced  
63 growth defect in Zn(II)-limited media and a lower bacterial burden in sepsis and pneumonia models  
64 of infection [4]. In addition to the ZnuABC permease, an outer membrane receptor, ZnuD1, and a  
65 Zn(II) metallochaperone, ZigA, have been shown to be necessary for *A. baumannii* survival in Zn(II)  
66 restricted conditions and infection in mice [4, 14]. Regulation of the Zn(II) acquisition machinery in  
67 *A. baumannii* is mediated by the Zn(II)-uptake regulator Zur, which belongs to the ferric uptake  
68 regulator (Fur) family of metalloregulators [15]. Zur mediates Zn(II)-dependent repression of the  
69 *znuABC*, *zigA*, and the *znuD1* pathways and thereby tightly regulates cellular abundance of Zn(II), in  
70 concert with metal ion-specific efflux pathways [16-18].

71           Here, we report the genomic, structural, and biochemical characterization of *A. baumannii*  
72 ZnuA. Amino acid sequence analyses indicated that the protein belongs to the Cluster A-I subgroup  
73 of SBPs associated with metal-specific prokaryotic ABC importers [19]. The structure of metal-free  
74 *A. baumannii* ZnuA revealed a canonical cluster A-I SBP fold, with molecular dynamics simulations  
75 predicting that loop  $\alpha 2\beta 2$ , which contains the metal-coordinating residue histidine (His) 41, to be  
76 highly mobile in the absence of Zn(II). By contrast, the other metal-coordinating His residues appear  
77 to comprise a relatively static preformed metal-binding site. Analysis of ZnuA mutant variants  
78 revealed the relative contribution of the histidine residues in SBP interaction and affinity for Zn(II).  
79 Collectively, these analyses provide the basis to propose a potential mechanism for Zn(II)-binding by  
80 *A. baumannii* ZnuA, which further expands our knowledge of the conformational landscape sampled  
81 by cluster A-I SBPs.

82

## 83 **2. MATERIALS AND METHODS**

### 84 **2.1 A. baumannii ZnuA sequence conservation within a global genomic framework**

85 A global diversity framework of 292 publicly available *A. baumannii* genome assemblies were  
86 derived from The PATRIC Bioinformatics Resource Center [20]. Sequence conservation and  
87 prevalence of *A. baumannii* AB5075\_UW (GenBank accession number: CP008706.1) gene products;  
88 ZnuA (ABUW\_3740), ZnuB (ABUW\_3743), ZnuC (ABUW\_3742), ZnuD1 (ABUW\_0600), ZigA  
89 (ABUW\_0073), ZuR (ABUW\_3741), GltA (ABUW\_0867), GyrB (ABUW\_0004), Cpn60  
90 (ABUW\_0918), RecA (ABUW\_1748), and RpoD (ABUW\_0862) were compared across the 292  
91 genomes using screen\_assembly v1.2.7 [21]. The search parameters used BLASTN v2.9.0 and were  
92 set to identify targets matching 80% sequence coverage and 80% sequence identity or above.  
93 Resulting hits were then translated into corresponding amino acid sequence. The sequence  
94 conservation of the analyzed genes was derived from a MUSCLE alignment [22] using Geneious  
95 prime [23] and the conservation percentages were derived from average pairwise identity.

### 97 **2.2 Expression and purification of recombinant ZnuA and mutant variants from inclusion** 98 **bodies**

99 Recombinant ZnuA (residues 20 – 268) was cloned from *A. baumannii* AB5075\_UW genomic DNA  
100 (ABUW\_3740) into pET-30a(+) vector via Gibson assembly. Mutant variants were generated using  
101 site-directed mutagenesis (QuickChange Lighting Kit, Agilent Technologies) using primers described  
102 in (**Table S1**). Wild-type ZnuA and mutant variants were overexpressed in *E. coli* LEMO21(DE3)  
103 with their respective expression construct (**Table S2**). Bacterial cultures were grown in Overnight  
104 Express Instant TB medium (Merck) supplemented with 10% glycerol and 100  $\mu\text{g}\cdot\text{mL}^{-1}$  kanamycin  
105 for 18 h at 26 °C. Cultures were harvested through centrifugation at 6,000  $\times g$  for 30 min, and pellets  
106 were resuspended in 50 mM 3-(*N*-morpholino)propanesulfonic acid (MOPS) (pH 7.8), 200 mM  
107 NaCl, 20% glycerol, and 15 mM imidazole buffer. Cells were homogenized and then lysed using  
108 mechanical disruption at 30 kpsi in a cell disruptor (Constant Systems) and were centrifugated at

109 120,000 × *g* at 4 °C for 1 h to isolate cellular debris. Cellular debris containing the inclusion bodies  
110 was then washed twice with washing buffer A (50 mM MOPS [pH 7.8], 2 M urea, 200 mM NaCl, 1  
111 mM ethylenediaminetetraacetic acid (EDTA), 1% Triton), and twice with washing buffer B (50 mM  
112 MOPS [pH 7.8], 200 mM NaCl, 1 mM EDTA) via centrifugation at 6,000 × *g* for 10 min. The  
113 supernatant was then discarded, and the pellets were stored at – 80 °C for future experiments.  
114 Inclusion bodies were solubilized in urea buffer A (50 mM MOPS [pH 7.8], 8 M urea, 200 mM NaCl)  
115 overnight with agitation at room temperature. The mixture was harvested by centrifugation at 120,000  
116 × *g* at 4 °C for 1 h, followed by filtration through a 0.4 μm filter (Sartorius). Dodecahistidine-tagged  
117 ZnuA recovered from the inclusion bodies was purified under denaturing conditions by immobilized  
118 metal ion affinity chromatography (IMAC) as described previously [24].

119

### 120 **2.3 Refolding of purified denatured ZnuA proteins and cleavage of dodecahistidine tag**

121 Purified, denatured wild-type and variant ZnuA proteins were refolded by dialysis in refolding buffer  
122 (50 mM MOPS, 0.25 M L-arginine, 500 mM NaCl, 1 mM EDTA) using a 20 kDa molecular weight-  
123 cutoff (MWCO) membrane (Slide-A-Lyzer, ThermoFisher Scientific) for 24 h at 4 °C. Insoluble  
124 material was removed from the refolded, recombinant ZnuA proteins by ultracentrifugation, 120,000  
125 × *g* at 4 °C for 1 h. The dodecahistidine tag was removed by enzymatic digestion using a recombinant  
126 histidine-tagged human rhinovirus 3C protease for 1 h at a ratio of 1:20 protease to recombinant ZnuA  
127 proteins at 4 °C with stirring. The sample was reverse purified with recombinant, tag-cleaved ZnuA  
128 proteins eluted from a 5 mL HisTrap column (Cytiva). Removal of the dodecahistidine tag was  
129 confirmed by SDS-PAGE analyses.

130

### 131 **2.4 Differential scanning fluorimetry**

132 Metal-free, recombinant tag-cleaved ZnuA and ZnuA variants (10 μM) were incubated with 10-fold  
133 molar excess of the first-row transition metal ions [Mn(II), Fe(II), Co(II), Ni(II), Cu(II), Zn(II)] at  
134 room temperature in the presence of 5 × SYPRO Orange (ThermoFisher Scientific). Samples were

135 subjected to thermal unfolding and analyzed using QuantStudio Flex 7 Real-Time PCR system  
136 (ThermoFisher Scientific) at a heating rate of  $0.3\text{ }^{\circ}\text{C}\cdot\text{s}^{-1}$ . Fluorescence data were collected at excitation  
137 470 nm/emission 570 nm for buffer only, metals only, protein with and without metal treatment. After  
138 subtraction of background fluorescence of the buffer, the first derivative of the fluorescence data was  
139 determined and analyzed using GraphPad Prism (Version 8) to determine the inflection point of the  
140 melting transition ( $T_m$ ). The metal-free protein showed a minor species ( $46.0 \pm 3.0\text{ }^{\circ}\text{C}$ ) and a major  
141 species ( $53.7 \pm 1.2\text{ }^{\circ}\text{C}$ ), with the major species used to determine the  $\Delta T_m$ . Although clarification by  
142 ultracentrifugation and/or filtration prior to differential scanning fluorimetry (DSF) did not prevent  
143 the metal-free sample  $T_m$  complexity, addition of metals ions produced a single species. Data from at  
144 least three independent experiments were used to determine the  $\Delta T_m \pm \text{S.D.}$  of the wild-type ZnuA  
145 and ZnuA variants. Statistical significance was determined using one-way ANOVA using a Tukey  
146 post-test.

147

## 148 **2.5 Metal-binding experiments**

149 Metal-free ZnuA ( $30\text{ }\mu\text{M}$ ) was incubated with 10-fold molar excess of the first-row transition metal  
150 ions [Mn(II), Fe(II), Co(II), Ni(II), Cu(II), Zn(II)] for 1 h with agitation in a total of 2 mL at  $4\text{ }^{\circ}\text{C}$ .  
151 Metal-binding assays were performed in binding assay buffer ( $50\text{ mM MOPS [pH 7.8]}$ ,  $200\text{ mM}$   
152  $\text{NaCl}$ ). Following incubation, unbound metal ions were removed by buffer exchange into the binding  
153 assay buffer using a PD10 column (GE Healthcare). Solutions of metal-loaded recombinant ZnuA  
154 were prepared in  $3.5\% \text{ HNO}_3$  and boiled at  $98\text{ }^{\circ}\text{C}$  for 15 min. Samples were then centrifuged for 30  
155 min at  $20,000 \times g$ , and the supernatant was analyzed using inductively coupled plasma-mass  
156 spectrometry (ICP-MS) to determine the metal:protein molar ratio [25, 26].

157

## 158 **2.6 Competitive Zn(II) binding assays**

159 Affinity measurement experiments were conducted by measuring the fluorescence of Mag-Fura-2  
160 ( $150\text{ nM}$ ) (ThermoFisher Scientific) saturated with Zn(II) in response to titration of metal-free protein

161 at (excitation 340 nm/emission 510 nm), using the CLARIOstar Plus spectrophotometer (BMG  
162 Labtech) [11]. Five technical replicates were measured for each sample in a black half-volume 384-  
163 well microtiter plate (Greiner Bio One), using a Chelex-100 treated 50 mM MOPS (pH 7.8) 200 mM  
164 NaCl buffer. Fluorescence values were analyzed in GraphPad Prism (Version 8) by a one-site non-  
165 linear fit model, using the experimentally derived  $K_D$  of Mag-Fura-2 (47 nM) to derive the  $K_D$  for  
166 Zn(II) binding by ZnuA.

167

## 168 **2.7 Structure determination by X-ray crystallography**

169 Recombinant ZnuA was concentrated to approximately 10 mg.mL<sup>-1</sup> in centrifugal filter units (Amicon  
170 MWCO 30 kDa, Millipore). Crystals were obtained at 20 °C using the hanging drop vapor diffusion  
171 technique in 0.1 M citrate (pH 7.0), 30% (v/v) polyethylene glycol 6000, and 1 M LiCl. Crystals were  
172 mounted onto Cryoloops (Hampton Research) and briefly soaked in Paratone-N (Hampton Research)  
173 prior to flash-cooling in liquid nitrogen. X-ray diffraction data were collected at the Australian  
174 Synchrotron MX2 beamline [27]. Diffraction data were indexed and integrated using *XDS* [28] and  
175 scaled and merged using *Aimless* [29]. The structure was determined using the molecular replacement  
176 in *Phenix Phaser* [30], using a search model generated *in silico* by AlphaFold2 [31]. An initial model  
177 was built in *Phenix.AutoBuild* [32]. The following residues could not be modeled due to the lack of  
178 electron density and are presumably disordered: Ser33-Gln38, Ser153-Ser154 and Thr216-Gln221.  
179 The structures was refined iteratively using *Phenix.Refine* [33] and manually modified in *COOT* [34].  
180 The coordinates and structure factors have been deposited in the Protein Data Bank (PDB ID 7SHJ).

181

## 182 **2.8 Molecular dynamics simulations**

183 Chain A in the crystal structure of metal-free ZnuA was used as the starting structure for the  
184 simulations. All crystallographic waters and sodium were removed. The residues missing in the model  
185 were reconstructed using the ‘Builder’ tool in PyMol [35]. All His residues were protonated based on  
186 hydrogen bonding potential with surrounding residues. For all simulation systems, the protein was

187 placed in a rectangular box, solvated with water molecules and Na<sup>+</sup> ions were added to neutralize the  
188 charge on the protein. Additional Na<sup>+</sup> and Cl<sup>-</sup> ions were added to obtain a final ionic strength of 100  
189 mM NaCl. The system was energy-minimized using a steepest descent algorithm, followed by a 5-ns  
190 NVT run and a 5-ns NPT run where the protein backbone atoms were position-restrained (posre) with  
191 a force constant of 500 kJ mol<sup>-1</sup>.nm<sup>-2</sup>. The output from the NPT posre run was used as the starting  
192 structure for the production runs. Three independent simulations of 750 ns each were carried out using  
193 different seeds to generate starting velocities.

194 All simulations were carried out using the GROMACS package version 5.0.1 [36, 37] in  
195 conjunction with the GROMOS 54a7 force field [38] for protein and the simple point charge (SPC)  
196 model for water [39]. Simulations were carried out under periodic boundary conditions with at least  
197 1.2 nm between the protein and the box wall. For non-bonded interactions, the van der Waals and  
198 short-ranged interactions were treated using a Verlet scheme with cut-offs 1.0 nm and 1.2 nm,  
199 respectively. Long-range electrostatics were treated using a PME with grid spacing 0.16 and a cubic  
200 interpolation of 4. The LINCS constraints algorithm was used. Temperature was kept at 298 K using  
201 a V-rescale thermostat and a time constant of 0.1 ps. A separate coupling groups was used for the  
202 protein and water/ions. Pressure was kept at 1 bar using a Parrinello-Rahman barostat with isotropic  
203 coupling and a time constant of 2.0. Simulations were carried out using a 2-fs time step. Initial  
204 velocities were randomly assigned from Maxwellian distributions at 298 K. Configurations were  
205 saved every 100 ps for analysis. Analysis was carried out using GROMACS tools and the python  
206 library MDAnalysis [40]. Unless otherwise stated, only the last 250 ns of each trajectory was used  
207 for analysis and independent simulations for a given system were analyzed separately. All images  
208 were prepared using VMD [41]. Cluster analysis was carried out using the algorithm of Daura *et al.*  
209 [42], implemented in GROMACS tools. A backbone neighbor root-mean-square deviation (RMSD)  
210 cut-off of 2.5 Å was used. From each of the simulations, the most dominant conformation was used.

211

## 212 **2.9 Data availability**

213 The accession code for the structure deposited in the Protein Data Bank is 7SHJ.

## 214 3. RESULTS AND DISCUSSION:

### 215 3.1 ZnuA and the zinc acquisition machinery are conserved in *A. baumannii* species

216 The conservation and prevalence of *A. baumannii* ZnuA and the other components of the Zn(II)  
217 acquisition system were investigated within a global database of 292 genome sequences (**Table S3**).  
218 This was performed by comparing the amino acid sequences of the ABC permease components, ZnuA  
219 (ABUW\_3740), ZnuB (ABUW\_3743), and ZnuC (ABUW\_3742), the outer membrane receptor  
220 ZnuD1 (ABUW\_0600), the metallochaperone ZigA (ABUW\_0073), and the metalloregulator ZnuR  
221 (ABUW\_3741) from 292 publicly available *A. baumannii* genomes, which represents isolates from  
222 environmental and clinical niches [20]. This analysis revealed that the Zn(II) acquisition machinery  
223 as defined by carriage of all 6 genes were present in >98% of *A. baumannii* genomes and exhibited  
224 >97% amino acid conservation (**Table 1**). Notably, ZnuA had sequence conservation of 99.9%, which  
225 is comparable to the multilocus sequence typing proteins GltA (ABUW\_0867), GyrB  
226 (ABUW\_0004), Cpn60 (ABUW\_0918), RecA (ABUW\_1748), RpoD (ABUW\_0862) (**Table 1**).  
227 Intriguingly, although *A. baumannii* ZnuA is highly conserved within *A. baumannii* strains, it has  
228 relatively low sequence homology (<30%) to the structurally and functionally characterized members  
229 of the cluster A-I family of Zn(II)-specific SBPs. The protein is most closely related to ZnuA from  
230 *Yersinia pestis* (25.1% sequence identity across 338 amino acid residues) and *E. coli* (24.5% sequence  
231 identity across 318 amino acid residues) (**Fig. 1A**) [43, 44]. ZnuA orthologs typically coordinate a  
232 single Zn(II) ion at the metal-binding site via three Nε2 atoms, contributed His side chains, and an O  
233 atom, contributed by either a carboxylate residue or water molecule. Alignment of *A. baumannii*  
234 ZnuA with other Zn(II)-specific SBPs identified three putative histidine residues as being highly  
235 conserved, His41, His109, and His170 (**Fig. 1B**). These putative Zn(II)-coordinating His residues  
236 were also invariant, i.e. 100% conservation, in all *A. baumannii* species analyzed. However, no  
237 conserved carboxylate residue was identified in *A. baumannii* ZnuA by comparison with other cluster  
238 A-I SBPs. This may suggest that Zn(II) retains coordination with a water molecule at the metal-  
239 binding site, as observed for ZnuA from *Synechocystis* sp. [45], or that the coordinating carboxylate

240 residue is contributed by a distinct region not observed in other characterized structures. *A. baumannii*  
241 ZnuA also lacks a histidine-rich region, which is frequently observed in other Zn(II)-specific SBPs  
242 (**Fig. 1B**). This region has been implicated in aiding SBP sampling of bulk solvent for Zn(II) ions  
243 [45, 46], although the length varies considerably and can span from 12 residues [47] to 50 residues  
244 [48]. Nevertheless, some Zn(II) specific SBPs, such as *S. pneumoniae* AdcAII [49], also lack this  
245 region, suggesting that its presence is not a prerequisite for function.

246 Collectively, these findings show that the Zn acquisition machinery is highly conserved in  
247 diversity of *A. baumannii* genomes analyzed. Further, the amino acid conservation of ZnuA indicates  
248 that mutations are poorly tolerated, suggesting that these rarely confer beneficial properties, with  
249 respect to the physiological function in ligand binding and/or interaction with ZnuBC.

250

### 251 **3.2 *A. baumannii* ZnuA can interact with zinc and cobalt**

252 To further investigate *A. baumannii* ZnuA a recombinant C-terminal dodecahistidine-tagged variant  
253 that lacked the predicted signal peptide sequence was generated (ABUW\_3740; residues 20 to 268).  
254 Recombinant ZnuA was expressed, the C-terminal dodecahistidine-tag cleaved and the protein  
255 reverse-purified and analyzed by size-exclusion chromatography. The recombinant protein had an  
256 estimated a relative molecular mass of 28.5 kDa, which compared favorably to the theoretical mass  
257 for monomeric species of 29.9 kDa (**Fig. 2A,B**).

258 The interaction of recombinant, tag-cleaved *A. baumannii* ZnuA with the first-row *d*-block  
259 elements manganese (Mn), iron (Fe), cobalt (Co), nickel (Ni), copper (Cu), and Zn was then assessed  
260 by DSF [50]. Recombinant ZnuA showed significant increases in thermostability, as defined by the  
261 apparent melting transition ( $T_m$ ) temperature upon interaction with Co(II) and Zn(II) (**Table 2**). The  
262 *d*-block elements Mn(II), Fe(II), Ni(II) and Cu(II), were not observed to induce significant changes  
263 in protein thermostability (**Table 2**). A limitation of DSF analyses is that it does not directly measure  
264 metal-binding. Ligand-induced increases in thermostability are inferred to reflect the formation of a  
265 more stable complex and in cluster A-I SBPs are indicative of conformational changes. Therefore, to

266 complement the DSF analyses, we also performed *in vitro* metal-binding experiments, to ascertain  
267 which *d*-block elements could interact with *A. baumannii* ZnuA. Metal-free recombinant ZnuA was  
268 incubated with a 10-fold molar excess of each *d*-block element, followed by desalting, to remove  
269 unbound metal ions. Analysis of recombinant ZnuA showed that it bound  $1.07 \pm 0.4$  mole of Zn(II)  
270 per mol of protein (S.E.M.; **Fig. 2C**). Thus, the *in vitro* Zn(II) binding data are consistent with the  
271 observation of a single high-affinity site within the structure of *A. baumannii* ZnuA, while the DSF  
272 analyses support the inference that Zn(II) is the physiological ligand.

273         Recombinant ZnuA was also observed to bind sub-stoichiometric amounts of Fe(II), Co(II)  
274 and Ni(II) and an excess of Cu(II) (~ 1.5 mole Cu(II) per mole ZnuA). However, Fe(II), Ni(II) and  
275 Cu(II) were not associated with  $T_m$  changes in recombinant ZnuA. This may be due to inability of  
276 these metal ions to interact with the primary metal binding site, poor affinity of these cations for the  
277 metal binding site leading to dissociation during desalting, failure of the metal-protein interaction to  
278 induce a transition to a more stable metal-protein complex, or some combination thereof. The first  
279 inference is potentially supported, at least in part, by the molar excess of Cu(II) associated with ZnuA.  
280 The putative composition of the metal-binding site of *A. baumannii* ZnuA, comprised by three  
281 histidine residues, is rarely observed in Cu-coordinating structures within the PDB [51]. We speculate  
282 that some or all of the ZnuA-bound Cu(II) was adventitiously associated with surface exposed sulfur-  
283 containing residues, such as methionine 208 and cysteine 209. Although future experiments would  
284 be required to validate this inference, metal ions interacting with secondary sites on the surfaces of  
285 SBPs have been reported [52-54]. However, it is important to note that the role of these secondary  
286 metal ion interaction sites remains unclear, as they do not appear to facilitate entry of metal ions into  
287 the ABC transporter [54].

288         In this work, Co(II) was the only non-cognate metal observed to bind and induce a  $T_m$  shift.  
289 The sub-stoichiometric association of Co(II) with ZnuA in the metal binding assay suggests that the  
290 protein has a poor affinity for the metal and/or that the metal is incapable of inducing a transition to  
291 a closed SBP conformation. Irrespective of the mechanistic basis, access to the metal binding site by

292 bulk solvent could promote dissociation of Co(II) during the desalting step of the protein-metal  
293 quantitation analytical process. Despite the capacity of Co(II) to interact with *A. baumannii* ZnuA, it  
294 is unclear whether it could be transported by the ZnuBC transporter. Recent structural and  
295 mechanistic studies of the related metal-specific ABC permease PsaBC from *Streptococcus*  
296 *pneumoniae* revealed a putative metal-binding site within the translocation pathway that was crucial  
297 for cation import [55]. The transmembrane binding site was essential for cation translocation and  
298 appeared to employ coordination chemistry. This mechanism was suggested to prevent translocation  
299 of non-cognate cations, such as Co(II). The coordination site residues are conserved within *A.*  
300 *baumannii* ZnuB (Asp39 and His43), although whether it serves in cation selectivity remains to be  
301 determined. It is also important to note that the acquisition of ionic Co(II) in prokaryotes is primarily  
302 mediated by energy-coupling factor (ECF) transporters, a distinct subgroup of bacterial ABC  
303 transporters [56, 57]. The Co(II)-specific ECF transporters employ the integral membrane protein  
304 CbiN that confers specificity for Co(II) ions in the CbiMQO<sub>2</sub> transporter [56, 57]. Thus, under  
305 physiological conditions it is reasonable to speculate that CbiN scavenges labile Co(II), thereby  
306 reducing potential interaction with ZnuA. A further consideration is that within the context of host  
307 niches, it is highly unlikely Co(II) would compete with Zn(II) for *A. baumannii* ZnuA, as Co is  
308 predominantly present as the metal chelate cobalamin. Collectively, this combination of factors may  
309 have obviated evolutionary selective pressure to evolve a capacity to discriminate between Zn(II) and  
310 Co(II) ions in ZnuA. We next sought to characterize the structural properties of *A. baumannii* ZnuA.

311

### 312 **3.3 Structural analysis of *A. baumannii* ZnuA**

313 Recombinant *A. baumannii* ZnuA was used in crystallographic trials, with and without Zn(II). Despite  
314 multiple attempts, Zn(II)-bound ZnuA did not yield crystals of sufficient quality for X-ray diffraction.  
315 Nevertheless, crystals of metal-free ZnuA were obtained and diffraction data was collected to 2.1 Å  
316 resolution. Two ZnuA molecules are present in each asymmetrical unit. Residues 1, 37-45, 159-160,  
317 222-227 in chain A and 1, 37-45, 160-163, 192-193, 220-224 in chain B were not modelled due to

318 lack of interpretable electron density in those regions. Crystallographic and refinement statistics are  
319 summarized in **Table S4**. *A. baumannii* ZnuA adopts a canonical cluster A-I SBP fold that is  
320 comprised by two globular domains, henceforth referred to as the N- and C-terminal domains, that  
321 each contain a 4- $\alpha$ -helical bundle ( $\alpha$ 1-4,  $\alpha$ 6-9) with a 4-stranded  $\beta$ -sheet ( $\beta$ 1-4,  $\beta$ 5-8). The two  
322 domains are connected by a long helical linker ( $\alpha$ 5) (**Fig. 3**), with the metal binding site predicted to  
323 be located at the interface between the two domains. The putative Zn(II)-coordinating residue, His41,  
324 is predicted to be located in the amino-terminal (N-terminal) domain loop  $\alpha$ 2 $\beta$ 2, but could not be  
325 modelled due to poorly resolved electron density of this region. His109 is located at the base of the  
326 metal binding site contributed by a short loop, while His170 is in the C-terminal domain loop  $\alpha$ 6 $\beta$ 5  
327 (**Fig. 3**). The structure of *A. baumannii* ZnuA represents an open, metal-free conformation, wherein  
328 the putative metal binding site is fully exposed to bulk solvent.

329 *A. baumannii* ZnuA was then compared with crystal structures of open-state cluster A-I SBPs  
330 of *E. coli* ZnuA (PDB 2PS3) [43], *Salmonella enterica* ZnuA (PDB 2XH8) [58], *Synechocystis* 6803  
331 ZnuA (PDB 2OV1) [46], *Paracoccus denitrificans* AztC (PDB 5W56) [59], and *S. pneumoniae*  
332 AdcAII (PDBs 7LM5, 7LM6) [11] (**Fig. 4**). This analysis revealed that the proteins adopted similar  
333 conformations, with root mean square deviations of the C $\alpha$  protein backbones (C $\alpha$ -RMSD) not  
334 exceeding 3.0 Å (**Table S5**). However, distinct differences between *A. baumannii* ZnuA and the  
335 representative cluster A-I SBPs were observed. Notably, loop  $\alpha$ 2 $\beta$ 2 in the N-terminal domain, which  
336 harbors the putative Zn(II)-coordinating residue His41, is largely disordered, indicating that this loop  
337 has high mobility in the absence of a metal ligand. This observation contrasts starkly with metal-free  
338 ZnuA from other bacterial species, wherein loop  $\alpha$ 2 $\beta$ 2 frequently adopts a stabilized, but distinct  
339 conformation. The disorder observed for loop  $\alpha$ 2 $\beta$ 2 in structural analysis of *A. baumannii* ZnuA  
340 closely resembles observations of this region in AdcA and AdcAII, the Zn(II)-recruiting SBPs of  
341 *Streptococcus pneumoniae* [9, 11]. In *S. pneumoniae* AdcA, loop  $\alpha$ 2 $\beta$ 2 was predicted to be disordered  
342 in the absence of Zn(II)-binding [9], and could not be modelled in the His65 mutant of AdcAII [11].  
343 Loop  $\alpha$ 2 $\beta$ 2 in AdcA has been proposed to serve as a “trap-door” component of the metal-binding

344 mechanism and has a crucial role in controlling solvent access to the Zn(II)-binding site and Zn(II)  
345 uptake. Here, we speculate that loop  $\alpha 2\beta 2$  may serve a similar role in *A. baumannii* ZnuA. Binding  
346 of a Zn(II) ion by loop  $\alpha 2\beta 2$  would enable the position of the mobile region to be stabilized and, upon  
347 coordination of the Zn(II) by other binding site residues, enable conformational changes that reduce  
348 bulk solvent access to the metal-binding site. Substantial conformational diversity was also observed  
349 in the C-terminal domain of *A. baumannii* ZnuA. In contrast to almost all other cluster A-I SBPs  
350 structures in their metal-free states,  $\alpha 8$  in *A. baumannii* ZnuA is disordered. In addition,  $\alpha 7$  and the  
351 4-stranded  $\beta$ -sheet show an approximate 2.4 Å shift relative to the same structural elements in other  
352 SBP crystal structures. The domain-linking helix  $\alpha 6$  is also shorter than the comparable region  
353 observed in other cluster A-I SBPs with the region connecting the C-terminal domain, residues 150-  
354 156, forming a loop, as opposed to being part of the domain-linking helix observed in all other SBPs.  
355 Whether the shorter length of this helix has a mechanistic effect on Zn(II)-binding remains to be  
356 investigated. Overall, the structural analysis of *A. baumannii* ZnuA reveals further diversity and  
357 complexity within the conformational landscape of open-state metal-recruiting SBPs.

358 To gain further insight into the structure of *A. baumannii* ZnuA molecular dynamics (MD)  
359 simulations were performed. The missing sections of the crystal structure were modelled as follows:  
360 residues 37-45 and 222-227 (the missing section at the end of the domain-linking helix  $\alpha 5$ ), were  
361 modelled as loops; residues 156-162 was modelled as an  $\alpha$ -helix. The SBP with the reconstructed  
362 sections was then used as a starting point for three independent, 750-ns long MD simulations of which  
363 the last 250 ns of each simulation were used for analysis. In all three simulations, the overall fold of  
364 the protein remained stable (**Fig. 5A**) with an average C $\alpha$ -RMSD of 1.8 Å  $\pm$  0.1 with respect to the  
365 starting structure. As suggested by the crystal structure, domain-linking helix  $\alpha 5$  ends at 150 and the  
366 remaining residues before the  $\beta$ -strand form a loop. This structure is confirmed by the absence of  
367 stable hydrogen bonds in the main chain between 150 and 156. The analysis suggests that *A.*  
368 *baumannii* ZnuA is unlikely to employ a rotation of the C-terminal domain for ligand binding, as  
369 observed in *S. pneumoniae* PsaA [60]. In reconstructed ZnuA,  $\alpha 7$  was modelled as an  $\alpha$ -helix and

370 remained stable in two (of the three) simulations. In one simulation, the first turn (residues 228-230)  
371 unfolded, while residues 224-228 remained in helical form. In all simulations, the loop formed by  
372 residues 218-222 that connects the preceding  $\beta$ -strand to  $\alpha 7$  is mobile, such that it affects the position  
373 of  $\alpha 7$  with respect to the plane running along the domain linking helix. We speculate that this motion  
374 and the instability of structural elements within  $\alpha 7$  contributed to the lack of interpretable diffraction  
375 electron density within this region of the crystal structure.

376 The MD simulations also enable further investigation of the loops that contain the putative  
377 Zn(II)-coordinating His residues. Loop  $\alpha 2\beta 2$ , which contains His41, showed the highest mobility and  
378 samples various conformations (**Fig. 5B**). As a result, the position of His41 with respect to the central  
379 Zn(II)-binding site varied substantially over the course of the simulations (**Fig. S1**). We predict that  
380 the mobility of loop  $\alpha 2\beta 2$  would be reduced in the Zn(II)-bound state. The short loop that contains  
381 His109, and loop  $\alpha 6\beta 5$ , which contains His170, show less mobility and adopt the same dominant  
382 conformation in *A. baumannii* ZnuA (**Fig. 5B, Fig. S1**). Accordingly, the positions of His109 and  
383 His170 are relatively stable with respect to the Zn(II)-binding site. Further analysis showed that the  
384 solvent accessibility of these loops fluctuates around the respective values observed in the crystal  
385 structure. In summary, the MD simulations of reconstructed ZnuA indicate that the overall fold of the  
386 metal-free SBP is stable, but regions of mobility are present within it, such as loop  $\alpha 2\beta 2$ , and these  
387 may contribute to the ligand recruiting mechanism.

388

### 389 **3.4 Putative metal-binding site histidine residues are essential for ZnuA function**

390 The role(s) of the putative metal-coordinating residues were then investigated by generating ZnuA  
391 point mutants lacking one of the three histidine residues. The resultant ZnuA variants ZnuA<sub>H41A</sub>,  
392 ZnuA<sub>H109A</sub> and ZnuA<sub>H170A</sub> were expressed and purified using the framework established for wild-  
393 type recombinant, tag-cleaved ZnuA. The affinity of wild-type ZnuA and the mutant variants was  
394 then determined using a competitive binding assay. The derived  $K_D$  of recombinant ZnuA for Zn(II)  
395 was determined to be  $87 \pm 2$  nM (S.E.M.; **Table 3**). This value is within the range reported for other

396 Zn(II)-specific SBPs [9, 10, 61, 62]. The ZnuA variants all had reduced affinity for Zn(II), but the  
397 extent varied substantially (**Table 3**). The overall order of Zn(II) affinity observed for the proteins  
398 was  $ZnuA > ZnuA_{H109A} > ZnuA_{H41A} > ZnuA_{H170A}$  (highest to lowest).

399 The impact of the mutations on protein thermostability was next assessed by DSF analyses  
400 (**Table 4**). The *A. baumannii* ZnuA variant proteins showed a minor reduction in overall  
401 thermostability by comparison to the wild-type protein (**Table 2**), although this was only statistically  
402 significant for  $ZnuA_{H170A}$  ( $P$  value = 0.0226; one-way ANOVA with Tukey post-test). The results  
403 strongly suggest that the point mutations did not perturb global protein structure and that the variant  
404 proteins were stable for further investigation of protein-metal complex interactions. DSF analysis of  
405 the *A. baumannii* ZnuA variant proteins revealed that substitution of any of the metal-binding site  
406 histidine residue abrogated the Zn(II) and Co(II) induced  $T_m$  shifts observed in the wild-type protein  
407 (**Tables 2,4**). The results indicate that residues His41, His109, and His170 all serve crucial roles in  
408 the stabilization of the *A. baumannii* ZnuA-metal complex.

409 Given the disruption in thermostabilization of cognate ligand binding observed by DSF  
410 analyses, the recombinant ZnuA variants were analyzed for *in vitro* zinc-binding capacity to assess  
411 whether this was also perturbed by the loss of the binding-site His residues. We observed that  
412  $ZnuA_{H41A}$  was not impacted for Zn(II)-binding, whereas  $ZnuA_{H109A}$  and  $ZnuA_{H170A}$  showed  
413 significant reductions in Zn(II) binding capacity, relative to the wild-type protein (**Fig. 6**). When  
414 considered in the context of the MD simulation analyses, the DSF data suggest that the metal-binding  
415 site is partially preformed by His109 and His170, which are relatively static in the protein structure  
416 and exposed to bulk solvent. By contrast, we predict that the mobile  $\alpha 2\beta 2$  loop, which contains His41,  
417 is stabilized upon Zn(II)-binding. Thus, these findings suggest a Zn(II)-binding mechanism wherein  
418 His109 and His170 serve to stabilize Zn(II) interaction with the base of the metal-binding site, while  
419 His41, upon interaction of Zn(II), serves to reduce the mobility of loop  $\alpha 2\beta 2$ , closing it over the  
420 binding site and reducing access to bulk solvent. The crucial role of His41 in ZnuA function is also  
421 supported by phenotypic studies of *A. baumannii* ATCC 1797 [4]. That work showed ectopic

422 expression of the *znuA*<sub>His41A</sub> variant in the *A. baumannii* ATCC 1797  $\Delta znuA$  background was  
423 incapable of rescuing growth in Luria broth treated with 30  $\mu$ M *N,N,N',N'*-tetrakis(2-  
424 pyridinylmethyl)-1,2-ethanediamine (TPEN), a preferential Zn(II)-chelator [4]. However, whether  
425 this was due to reduced affinity of ZnuA variant for Zn(II), the inability to stabilize loop  $\alpha 2\beta 2$  and  
426 preventing TPEN chelation of bound Zn(II), and/or disruption of the ZnuA-ZnuBC interface, remains  
427 to be determined. Further investigations into the metal-binding dynamics of *A. baumannii* ZnuA and  
428 the structure of Zn(II)-bound wild-type SBP and mutant derivatives would address the veracity of  
429 this mechanistic model.  
430

431 **4. CONCLUSIONS**

432 This study provides new insights into the structure and mechanistic aspects of *A. baumannii* ZnuA.  
433 This Zn(II)-recruiting protein is a highly conserved component of the essential acquisition machinery  
434 present in diverse *A. baumannii* strains. The high-resolution structure of open, metal-free state of  
435 ZnuA reveals that the N-terminal loop  $\alpha 2\beta 2$ , which contains the Zn(II)-binding His41 residue, is a  
436 region of dynamic mobility in the absence of ligand. This region appears to play a crucial role in  
437 occluding Zn(II) at the metal-binding site from bulk solvent and thereby promotes efficacious import  
438 via the ZnuBC transporter. The essentiality of Zn(II) for bacterial pathogens makes it a highly  
439 attractive target for antimicrobial development. The data herein provides a foundation for future  
440 structure-based therapeutic development studies to target *A. baumannii* ZnuA-mediated Zn(II)  
441 acquisition.

442

## TABLES

**Table 1. Conservation and prevalence of known *A. baumannii* Zn(II) acquisition proteins within 292 genome sequences.**

<b>Zn(II) acquisition proteins</b>	<b>Conservation (%)</b>	<b>Prevalence (%)</b>
ABUW_3740 ( <b>ZnuA</b> )	99.9	99.3
ABUW_3743 ( <b>ZnuB</b> )	99.4	99.6
ABUW_3742 ( <b>ZnuC</b> )	99.6	99.6
ABUW_3741 ( <b>ZuR</b> )	99.9	100
ABUW_0600 ( <b>ZnuD1</b> )	97.9	98.2
ABUW_0073 ( <b>ZigA</b> )	99	98.9
<b>MLST proteins</b>	<b>Conservation (%)</b>	<b>Prevalence (%)</b>
ABUW_0876 ( <b>GltA</b> )	100	100
ABUW_1083 ( <b>GyrB</b> )	99.8	100
ABUW_0918 ( <b>Cpn60</b> )	100	100
ABUW_1748 ( <b>RecA</b> )	100	99.6
ABUW_0862 ( <b>RpoD</b> )	100	100

**Table 2. Effect of divalent cations on the melting temperature of wild type ZnuA**

<b>Metal Treatment</b>	<b><math>T_m</math> (°C)<sup>†</sup></b>	<b><math>\Delta T_m</math></b>
Metal-free ZnuA	55.5 ± 1.2	
ZnuA 1:10 Mn(II)	55.3 ± 0.9	- 0.2
ZnuA 1:10 Fe(II)	53.8 ± 0.9	- 1.7
ZnuA 1:10 Co(II)	58.8 ± 1.3	+ 3.3 <sup>‡</sup>
ZnuA 1:10 Ni(II)	57.4 ± 0.5	+ 1.9
ZnuA 1:10 Cu(II)	55.3 ± 1.9	- 0.2
ZnuA 1:10 Zn(II)	63.8 ± 0.8	+ 8.3 <sup>‡</sup>

<sup>†</sup> Values shown represent the mean and standard deviation from at least three independent measurements.

<sup>‡</sup> Statistically significant difference compared to metal-free protein  $T_m$  (one-way ANOVA with Tukey post-test).

**Table 3. Effect of metal binding site mutations on *in vitro* Zn(II) binding**

<b>Protein</b>	<b><math>K_D</math> (nM)</b>
ZnuA	$87 \pm 2$
ZnuA <sub>H41A</sub>	$342 \pm 125$
ZnuA <sub>H109A</sub>	$114 \pm 33$
ZnuA <sub>H170A</sub>	$658 \pm 103$

**Table 4. Effect of divalent cations on the melting temperature of ZnuA variant proteins**

<b>Metal Treatment</b>	<b>ZnuA<sub>H41A</sub></b> $T_m$ (°C) <sup>†</sup>	<b>ZnuA<sub>H41A</sub></b> $\Delta T_m$	<b>ZnuA<sub>H109A</sub></b> $T_m$ (°C) <sup>†</sup>	<b>ZnuA<sub>H109A</sub></b> $\Delta T_m$	<b>ZnuA<sub>H170A</sub></b> $T_m$ (°C) <sup>†</sup>	<b>ZnuA<sub>H170A</sub></b> $\Delta T_m$
Metal-free ZnuA	53.5 ± 0.1		53.2 ± 0.1		52.7 ± 0.4	
ZnuA 1:10 Mn(II)	54.3 ± 1.0	+ 0.8	52.1 ± 0.8	- 1.1	52.5 ± 0.6	- 0.2
ZnuA 1:10 Fe(II)	55.0 ± 0.2	+ 1.5	52.4 ± 0.5	- 0.8	53.1 ± 0.6	+ 0.4
ZnuA 1:10 Co(II)	54.8 ± 1.1	+ 1.3	52.9 ± 0.7	- 0.3	52.9 ± 0.5	+ 0.2
ZnuA 1:10 Ni(II)	56.3 ± 0.4	+ 2.8 <sup>‡</sup>	53.3 ± 0.7	+ 0.1	53.7 ± 0.1	+ 1.0
ZnuA 1:10 Cu(II)	52.5 ± 0.8	- 1.0	52.4 ± 0.4	- 0.8	52.0 ± 0.0	- 0.7
ZnuA 1:10 Zn(II)	55.2 ± 1.2	+ 1.7	54.4 ± 1.8	+ 1.2	51.9 ± 3.5	- 0.8

<sup>†</sup> Values shown represent the mean and standard deviation from at least three independent measurements.

<sup>‡</sup> Statistically significant difference compared to metal-free protein  $T_m$  (one-way ANOVA with Tukey post-test).

## FIGURE LEGENDS

### Figure 1. Sequence homology and alignment of *A. baumannii* ZnuA in comparison to cluster A-I Zn(II) SBPs

(A) Sequence percentage identity of characterized cluster A-I Zn(II) SBPs, compared to *A. baumannii* ZnuA. The numbers inside the boxes represent the sequence identity percentage. (B) Sequence comparison and alignment between *A. baumannii* ZnuA and Zn(II)-binding cluster A-I SBPs. The conserved His residues are highlighted in green and the His-rich loop highlighted in blue.

### Figure 2. Purification of recombinant wild-type ZnuA from inclusion bodies

(A) Absorbance (280 nm) trace of recombinant ZnuA, analyzed by size exclusion chromatography using a Superdex 200 increase 10/300 GL column. The inset represents linear regression of protein molecular weight standard calibration. (B) Coomassie-stained 12.5% SDS-PAGE showing: lane 1, molecular weight standards with sizes indicated (left); and lane 2, peak eluent fraction from size exclusion column (A) with ZnuA indicated by an arrow. (C) *In vitro* metal-binding experiments of the metal-free ZnuA with *d*-block metal ions shown. Data represent the mean molar ratio of metal ions to ZnuA ( $\pm$  S.E.M.) from at least three independent biological experiments.

### Figure 3. Crystal structure of *A. baumannii* ZnuA in the metal-free state

The structure of metal-free ZnuA (PDB ID 7SHJ) with the N- and C-terminal domains colored in green and yellow, respectively, and the domain-linking helix in magenta. The Zn(II)-coordinating residues His109 and His170 are shown in stick representation.

### Figure 4. Structural comparisons of *A. baumannii* ZnuA with homologues in their metal-free states

Structural comparison of *A. baumannii* ZnuA (magenta) with (A) *E. coli* ZnuA (PDB ID 2PS3; yellow); (B) *S. enterica* ZnuA (PDB ID 2XH8; cyan); (C) *Synechocystis* 6803 ZnuA (PDB ID 2OV1;

light blue); (D) *P. denitrificans* AztC (PDB ID 5W56; grey); (E) *S. pneumoniae* AdcAII<sub>H65A</sub> (PDB ID 7LM5; light green); and (F) *S. pneumoniae* AdcAII<sub>H205L</sub> (PDB ID 7LM6; orange). The metal-coordinating residues of the respective structure are shown in stick representation. The  $\alpha 2\beta 2$  loop (denoted by arrow) and  $\alpha 8$  regions, which are absent in the *A. baumannii* ZnuA crystal structure, and  $\alpha 7$ , which shifts relative to the same structural elements in other structures, are labeled.

### Figure 5. MD simulations of reconstructed ZnuA

(A) Overlay of the metal-free ZnuA structure (PDB ID 7SHJ; magenta) with a representative structure from MD simulations of the reconstructed metal-free ZnuA structure (cyan). (B) MD simulations examining the mobility of the histidine-containing loops. A representative structure of the full-length, reconstructed ZnuA structure is shown in cyan and overlaid with 12 conformations of loops from the MD simulations:  $\alpha 2\beta 2$ , which contains His41, shown in red; the short loop containing His109 shown in blue; and  $\alpha 6\beta 5$ , which contains His170, shown in orange.

### Figure 6. *In vitro* Zn(II) binding of wild-type ZnuA and mutant variants

*In vitro* Zn(II)-binding experiments of ZnuA and the mutant variants ZnuA<sub>H41A</sub>, ZnuA<sub>H109A</sub>, ZnuA<sub>H170A</sub>. Data represent the mean molar ratio of <sup>66</sup>Zn to protein ( $\pm$  S.E.M.) from at least three independent biological experiments. Statistical significance was determined by performing a one-way ANOVA analysis with Bonferroni post-test.

## **ACKNOWLEDGEMENTS**

We thank Dr Bart Eijkelkamp (Flinders University, Australia) for providing the AB5075\_UW strain and for discussions. We also thank Prof. Eric Skaar and Laura Hesse (Vanderbilt University, USA) for discussions and feedback on the manuscript. We acknowledge use and thank the staff of the Australian Synchrotron MX beamlines and the UQ-ROCX (University of Queensland Remote Operation Crystallization and X-Ray Diffraction) Australian Microscopy & Microanalysis Research Facility at the Centre for Microscopy and Microanalysis, The University of Queensland.

## **FUNDING**

This research was undertaken with the assistance of resources and services from the National Computational Infrastructure (NCI), which is supported by the Australian Government and by resources provided by The Pawsey Supercomputing Centre with funding from the Australian Government and the Government of Western Australia. This research was also undertaken using the LIEF HPC-GPGPU Facility hosted at the University of Melbourne. This Facility was established with the assistance of Australian Research Council (ARC) LIEF Grant LE170100200. This work was supported by the National Health and Medical Research Council (NHMRC) grants 1071659 to B.K., 1122582 to C.A.M., and 1180826 to B.K. and C.A.M. E.D. is a UTS Chancellor's Postdoctoral Fellow, B.K. is an ARC Laureate Fellow (FL180100109), and C.A.M. is an ARC Future Fellow (FT170100006). The content of this study is solely the responsibility of the authors and does not necessarily represent the official views of the funding bodies.

## **AUTHOR CONTRIBUTIONS**

SA, MRD, BK, ED, and CAM designed the study. SA performed the biochemical and biophysical studies, with KG performing the ICP-MS analyses. SA, AH, and MRD performed the bioinformatic studies. ZL, TV, and BK performed the structural analyses. ED and SIH performed the molecular dynamics studies. SA wrote the first draft of the manuscript with specific sections contributed by ZL

and ED. CAM reviewed and revised the manuscript text. All authors read and approved the submitted version.

## REFERENCES

- [1] C. Andreini, L. Banci, I. Bertini, A. Rosato, *J Proteome Res*, vol. 5, 2006, pp. 3173-3178.
- [2] C. Andreini, I. Bertini, G. Cavallaro, G.L. Holliday, J.M. Thornton, *J Biol Inorg Chem*, vol. 13, 2008, pp. 1205-1218.
- [3] K. Hantke, *Curr Opin Microbiol*, vol. 8, 2005, pp. 196-202.
- [4] L.E. Hesse, Z.R. Lonergan, W.N. Beavers, E.P. Skaar, *Infect Immun*, vol. 87, 2019, pp. e00746-00719.
- [5] S. Lhospice, N.O. Gomez, L. Ouerdane, C. Brutesco, G. Ghssein, C. Hajjar, A. Liratni, S. Wang, P. Richaud, S. Bleves, G. Ball, E. Borezee-Durant, R. Lobinski, D. Pignol, P. Arnoux, R. Voulhoux, *Sci Rep*, vol. 7, 2017, pp. 17132.
- [6] V.G. Pederick, B.A. Eijkelkamp, S.L. Begg, M.P. Ween, L.J. McAllister, J.C. Paton, C.A. McDevitt, *Sci Rep*, vol. 5, 2015, pp. 13139.
- [7] R. Gabbianelli, R. Scotti, S. Ammendola, P. Petrarca, L. Nicolini, A. Battistoni, *BMC Microbiol*, vol. 11, 2011, pp. 36.
- [8] S. Ammendola, P. Pasquali, C. Pistoia, P. Petrucci, P. Petrarca, G. Rotilio, A. Battistoni, *Infect Immun*, vol. 75, 2007, pp. 5867-5876.
- [9] Z. Luo, J.R. Morey, E. Deplazes, A. Motygullina, A. Tan, K. Ganio, S.L. Neville, N. Eleftheriadis, M. Isselstein, V.G. Pederick, J.C. Paton, T. Cordes, J.R. Harmer, B. Kobe, C.A. McDevitt, *mBio*, vol. 12, 2021, pp. e01958-01920.
- [10] C.D. Plumptre, B.A. Eijkelkamp, J.R. Morey, F. Behr, R.M. Counago, A.D. Ogunniyi, B. Kobe, M.L. O'Mara, J.C. Paton, C.A. McDevitt, *Mol Microbiol*, vol. 91, 2014, pp. 834-851.
- [11] M.L. Zupan, Z. Luo, K. Ganio, V.G. Pederick, S.L. Neville, E. Deplazes, B. Kobe, C.A. McDevitt, *Front Cell Infect Microbiol*, vol. 11, 2021, pp. 729981.
- [12] E. Tacconelli, E. Carrara, A. Savoldi, S. Harbarth, M. Mendelson, D.L. Monnet, C. Pulcini, G. Kahlmeter, J. Kluytmans, Y. Carmeli, M. Ouellette, K. Outtersson, J. Patel, M. Cavaleri, E.M. Cox,

- C.R. Houchens, M.L. Grayson, P. Hansen, N. Singh, U. Theuretzbacher, N. Magrini, W.H.O.P.P.L.W. Group, *Lancet Infect Dis*, vol. 18, 2018, pp. 318-327.
- [13] M.I. Hood, B.L. Mortensen, J.L. Moore, Y. Zhang, T.E. Kehl-Fie, N. Sugitani, W.J. Chazin, R.M. Caprioli, E.P. Skaar, *PLoS Pathog*, vol. 8, 2012, pp. e1003068.
- [14] B.L. Nairn, Z.R. Lonergan, J. Wang, J.J. Braymer, Y. Zhang, M.W. Calcutt, J.P. Lisher, B.A. Gilston, W.J. Chazin, V. de Crecy-Lagard, D.P. Giedroc, E.P. Skaar, *Cell Host Microbe*, vol. 19, 2016, pp. 826-836.
- [15] B.L. Mortensen, S. Rathi, W.J. Chazin, E.P. Skaar, *J Bacteriol*, vol. 196, 2014, pp. 2616-2626.
- [16] S.F. Alquethamy, F.G. Adams, V. Naidu, M. Khorvash, V.G. Pederick, M. Zang, J.C. Paton, I.T. Paulsen, K.A. Hassan, A.K. Cain, C.A. McDevitt, B.A. Eijkelkamp, *ACS Infect Dis*, vol. 6, 2020, pp. 150-158.
- [17] S.F. Alquethamy, M. Khorvash, V.G. Pederick, J.J. Whittall, J.C. Paton, I.T. Paulsen, K.A. Hassan, C.A. McDevitt, B.A. Eijkelkamp, *Int J Mol Sci*, vol. 20, 2019, pp. 575.
- [18] S.F. Alquethamy, F.G. Adams, R. Maharjan, N.N. Delgado, M. Zang, K. Ganio, J.C. Paton, K.A. Hassan, I.T. Paulsen, C.A. McDevitt, A.K. Cain, B.A. Eijkelkamp, *Appl Environ Microbiol*, vol. 87, 2021, pp. e0171821.
- [19] G.H. Scheepers, A.N.J.A. Lycklama, B. Poolman, *FEBS Lett*, vol. 590, 2016, pp. 4393-4401.
- [20] J.J. Davis, A.R. Wattam, R.K. Aziz, T. Brettin, R. Butler, R.M. Butler, P. Chlenski, N. Conrad, A. Dickerman, E.M. Dietrich, J.L. Gabbard, S. Gerdes, A. Guard, R.W. Kenyon, D. Machi, C. Mao, D. Murphy-Olson, M. Nguyen, E.K. Nordberg, G.J. Olsen, R.D. Olson, J.C. Overbeek, R. Overbeek, B. Parrello, G.D. Pusch, M. Shukla, C. Thomas, M. VanOeffelen, V. Vonstein, A.S. Warren, F. Xia, D. Xie, H. Yoo, R. Stevens, *Nucleic Acids Res*, vol. 48, 2020, pp. D606-D612.
- [21] M.R. Davies, L. McIntyre, A. Mutreja, J.A. Lacey, J.A. Lees, R.J. Towers, S. Duchene, P.R. Smeesters, H.R. Frost, D.J. Price, M.T.G. Holden, S. David, P.M. Giffard, K.A. Worthing, A.C. Seale, J.A. Berkley, S.R. Harris, T. Rivera-Hernandez, O. Berking, A.J. Cork, R. Torres, T. Lithgow, R.A. Strugnell, R. Bergmann, P. Nitsche-Schmitz, G.S. Chhatwal, S.D. Bentley, J.D.

- Fraser, N.J. Moreland, J.R. Carapetis, A.C. Steer, J. Parkhill, A. Saul, D.A. Williamson, B.J. Currie, S.Y.C. Tong, G. Dougan, M.J. Walker, *Nat Genet*, vol. 51, 2019, pp. 1035-1043.
- [22] R.C. Edgar, *Nucleic Acids Res*, vol. 32, 2004, pp. 1792-1797.
- [23] M. Kearse, R. Moir, A. Wilson, S. Stones-Havas, M. Cheung, S. Sturrock, S. Buxton, A. Cooper, S. Markowitz, C. Duran, T. Thierer, B. Ashton, P. Meintjes, A. Drummond, *Bioinformatics*, vol. 28, 2012, pp. 1647-1649.
- [24] M.Y. Linova, M.W. Risor, S.E. Jorgensen, Z. Mansour, J. Kaya, J.J. Sigurdarson, J.J. Enghild, H. Karring, *Protein Expr Purif*, vol. 166, 2020, pp. 105507.
- [25] E.B. Brazel, A. Tan, S.L. Neville, A.R. Iverson, S.R. Udagedara, B.A. Cunningham, M. Sikanyika, D.M.P. De Oliveira, B. Keller, L. Bohlmann, I.M. El-Deeb, K. Ganio, B.A. Eijkelkamp, A.G. McEwan, M. von Itzstein, M.J. Maher, M.J. Walker, J.W. Rosch, C.A. McDevitt, *Cell Rep*, vol. 38, 2022, pp. 110202.
- [26] S.L. Neville, B.A. Eijkelkamp, A. Lothian, J.C. Paton, B.R. Roberts, J.W. Rosch, C.A. McDevitt, *Commun Biol*, vol. 3, 2020, pp. 694.
- [27] T.M. McPhillips, S.E. McPhillips, H.J. Chiu, A.E. Cohen, A.M. Deacon, P.J. Ellis, E. Garman, A. Gonzalez, N.K. Sauter, R.P. Phizackerley, S.M. Soltis, P. Kuhn, *J Synchrotron Radiat*, vol. 9, 2002, pp. 401-406.
- [28] W. Kabsch, *Acta Crystallogr D Biol Crystallogr*, vol. 66, 2010, pp. 125-132.
- [29] P.R. Evans, G.N. Murshudov, *Acta Crystallogr D Biol Crystallogr*, vol. 69, 2013, pp. 1204-1214.
- [30] P.D. Adams, P.V. Afonine, G. Bunkoczi, V.B. Chen, I.W. Davis, N. Echols, J.J. Headd, L.W. Hung, G.J. Kapral, R.W. Grosse-Kunstleve, A.J. McCoy, N.W. Moriarty, R. Oeffner, R.J. Read, D.C. Richardson, J.S. Richardson, T.C. Terwilliger, P.H. Zwart, *Acta Crystallogr D Biol Crystallogr*, vol. 66, 2010, pp. 213-221.
- [31] J. Jumper, R. Evans, A. Pritzel, T. Green, M. Figurnov, O. Ronneberger, K. Tunyasuvunakool, R. Bates, A. Zidek, A. Potapenko, A. Bridgland, C. Meyer, S.A.A. Kohl, A.J. Ballard, A. Cowie, B.

- Romera-Paredes, S. Nikolov, R. Jain, J. Adler, T. Back, S. Petersen, D. Reiman, E. Clancy, M. Zielinski, M. Steinegger, M. Pacholska, T. Berghammer, S. Bodenstein, D. Silver, O. Vinyals, A.W. Senior, K. Kavukcuoglu, P. Kohli, D. Hassabis, *Nature*, vol. 596, 2021, pp. 583-589.
- [32] T.C. Terwilliger, R.W. Grosse-Kunstleve, P.V. Afonine, N.W. Moriarty, P.H. Zwart, L.W. Hung, R.J. Read, P.D. Adams, *Acta Crystallogr D Biol Crystallogr*, vol. 64, 2008, pp. 61-69.
- [33] P.V. Afonine, R.W. Grosse-Kunstleve, N. Echols, J.J. Headd, N.W. Moriarty, M. Mustyakimov, T.C. Terwilliger, A. Urzhumtsev, P.H. Zwart, P.D. Adams, *Acta Crystallogr D Biol Crystallogr*, vol. 68, 2012, pp. 352-367.
- [34] P. Emsley, B. Lohkamp, W.G. Scott, K. Cowtan, *Acta Crystallogr D Biol Crystallogr*, vol. 66, 2010, pp. 486-501.
- [35] L. Schrödinger, W. DeLano, <http://www.pymol.org/pymol>, 2020.
- [36] M.J. Abraham, T. Murtola, R. Schulz, S. Páll, J.C. Smith, B. Hess, E. Lindahl, *SoftwareX*, vol. 1-2, 2015, pp. 19-25.
- [37] Lindahl., Abraham., Hess., V.d. Spoel., Zenodo, 2020.
- [38] N. Schmid, A.P. Eichenberger, A. Choutko, S. Riniker, M. Winger, A.E. Mark, W.F. van Gunsteren, *Eur Biophys J*, vol. 40, 2011, pp. 843-856.
- [39] P.J.P.M. Berendsen H.J.C, van Gunsteren W.F, Hermans J, *Intermolecular Forces*, vol. 14, 1981, pp. 331-342.
- [40] N. Michaud-Agrawal, E.J. Denning, T.B. Woolf, O. Beckstein, *J Comput Chem*, vol. 32, 2011, pp. 2319-2327.
- [41] W. Humphrey, A. Dalke, K. Schulten, *J Mol Graph*, vol. 14, 1996, pp. 33-38, 27-38.
- [42] X. Daura, K. Gademann, B. Jaun, D. Seebach, W.F. van Gunsteren, A.E. Mark, *Angew Chem Int Ed*, vol. 38, 1999, pp. 236-240.
- [43] L.A. Yatsunyk, J.A. Easton, L.R. Kim, S.A. Sugarbaker, B. Bennett, R.M. Breece, Vorontsov, II, D.L. Tierney, M.W. Crowder, A.C. Rosenzweig, *J Biol Inorg Chem*, vol. 13, 2008, pp. 271-288.

- [44] D.C. Desrosiers, S.W. Bearden, I. Mier, Jr., J. Abney, J.T. Paulley, J.D. Fetherston, J.C. Salazar, J.D. Radolf, R.D. Perry, *Infect Immun*, vol. 78, 2010, pp. 5163-5177.
- [45] S. Banerjee, B. Wei, M. Bhattacharyya-Pakrasi, H.B. Pakrasi, T.J. Smith, *J Mol Biol*, vol. 333, 2003, pp. 1061-1069.
- [46] B. Wei, A.M. Randich, M. Bhattacharyya-Pakrasi, H.B. Pakrasi, T.J. Smith, *Biochemistry*, vol. 46, 2007, pp. 8734-8743.
- [47] D.C. Desrosiers, Y.C. Sun, A.A. Zaidi, C.H. Eggers, D.L. Cox, J.D. Radolf, *Mol Microbiol*, vol. 65, 2007, pp. 137-152.
- [48] D. Lu, B. Boyd, C.A. Lingwood, *J Biol Chem*, vol. 272, 1997, pp. 29033-29038.
- [49] E. Loisel, L. Jacquamet, L. Serre, C. Bauvois, J.L. Ferrer, T. Vernet, A.M. Di Guilmi, C. Durmort, *J Mol Biol*, vol. 381, 2008, pp. 594-606.
- [50] F.H. Niesen, H. Berglund, M. Vedadi, *Nat Protoc*, vol. 2, 2007, pp. nprot.2007.2321.
- [51] V. Putignano, A. Rosato, L. Banci, C. Andreini, *Nucleic Acids Res*, vol. 46, 2018, pp. D459-D464.
- [52] B. Zheng, Q. Zhang, J. Gao, H. Han, M. Li, J. Zhang, J. Qi, J. Yan, G.F. Gao, *PLoS One*, vol. 6, Public Library of Science, 2011, pp. e19510.
- [53] A. Hecel, A. Kola, D. Valensin, H. Kozlowski, M. Rowinska-Zyrek, *Inorg Chem*, vol. 59, American Chemical Society, 2020, pp. 1947-1958.
- [54] C.D. Radka, S.G. Aller, *Acta Crystallogr F Struct Biol Commun*, vol. 77, 2021, pp. 286-293.
- [55] S.L. Neville, J. Sjöhamn, J.A. Watts, H. MacDermott-Opeskin, S.J. Fairweather, K. Ganio, A. Carey Hulyer, A.P. McGrath, A.J. Hayes, T.R. Malcolm, M.R. Davies, N. Nomura, S. Iwata, M.L. O'Mara, M.J. Maher, C.A. McDevitt, *Sci Adv*, vol. 7, 2021.
- [56] S. Siche, O. Neubauer, P. Hebbeln, T. Eitinger, *Res Microbiol*, vol. 161, 2010, pp. 824-829.
- [57] F. Finkenwirth, M. Sippach, S.N. Pecina, M. Gade, J. Ruta, A. Ricke, E. Bondarenko, J.P. Klare, M. Zinke, S. Lange, A. Lange, H.J. Steinhoff, T. Eitinger, *Biochim Biophys Acta Biomembr*, vol. 1862, 2020, pp. 183114.

[58] A. Ilari, F. Alaleona, P. Petrarca, A. Battistoni, E. Chiancone, *J Mol Biol*, vol. 409, 2011, pp. 630-641.

[59] D.P. Neupane, D. Avalos, S. Fullam, H. Roychowdhury, E.T. Yukl, *J Biol Chem*, vol. 292, 2017, pp. 17496-17505.

[60] R.M. Couñago, M.P. Ween, S.L. Begg, M. Bajaj, J. Zuegg, M.L. O'Mara, M.A. Cooper, A.G. McEwan, J.C. Paton, B. Kobe, C.A. McDevitt, *Nat Chem Biol*, vol. 10, 2014, pp. 35-41.

[61] M. Handali, H. Roychowdhury, D.P. Neupane, E.T. Yukl, *J Biol Chem*, vol. 290, 2015, pp. 29984-29992.

[62] Y.M. Lee, C. Lim, *J Mol Biol*, vol. 379, 2008, pp. 545-553.

## Table of Abbreviations

*A. baumannii*, *Acinetobacter baumannii*

ABC, ATP-binding cassette

C $\alpha$ , alpha carbon

CDC, Centers for Disease Control and Prevention

DSF, differential scanning fluorimetry

ECF, energy-coupling factor

EDTA, ethylenediaminetetraacetic acid

*E. coli*, *Escherichia coli*

His, histidine

ICP-MS, inductively coupled plasma-mass spectrometry

IMAC, immobilized metal ion affinity chromatography

MD, molecular dynamics

MOPS, 3-(*N*-morpholino)propanesulfonic acid

MWCO, molecular weight cutoff

N-terminal, amino-terminal

*P. denitrificans*, *Paracoccus denitrificans*

RMSD, root mean square deviation

SBP, solute-binding protein

SDS-PAGE, sodium dodecyl sulfate–polyacrylamide gel electrophoresis

S.E.M., standard error of the mean

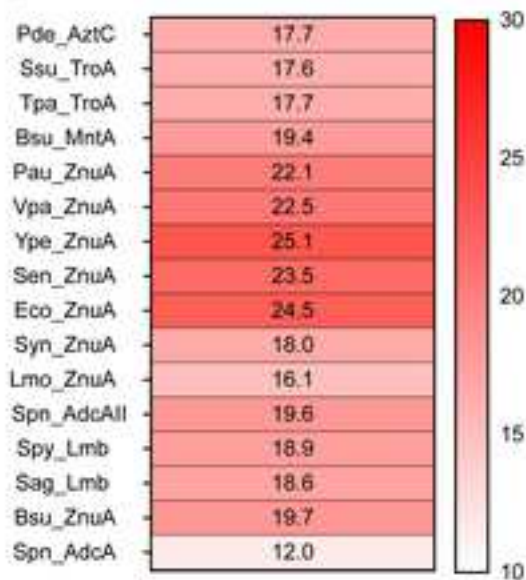
*S. enterica*, *Salmonella enterica*

*S. pneumoniae*, *Streptococcus pneumoniae*

TPEN, *N,N,N',N'*-tetrakis(2-pyridinylmethyl)-1,2-ethanediamine

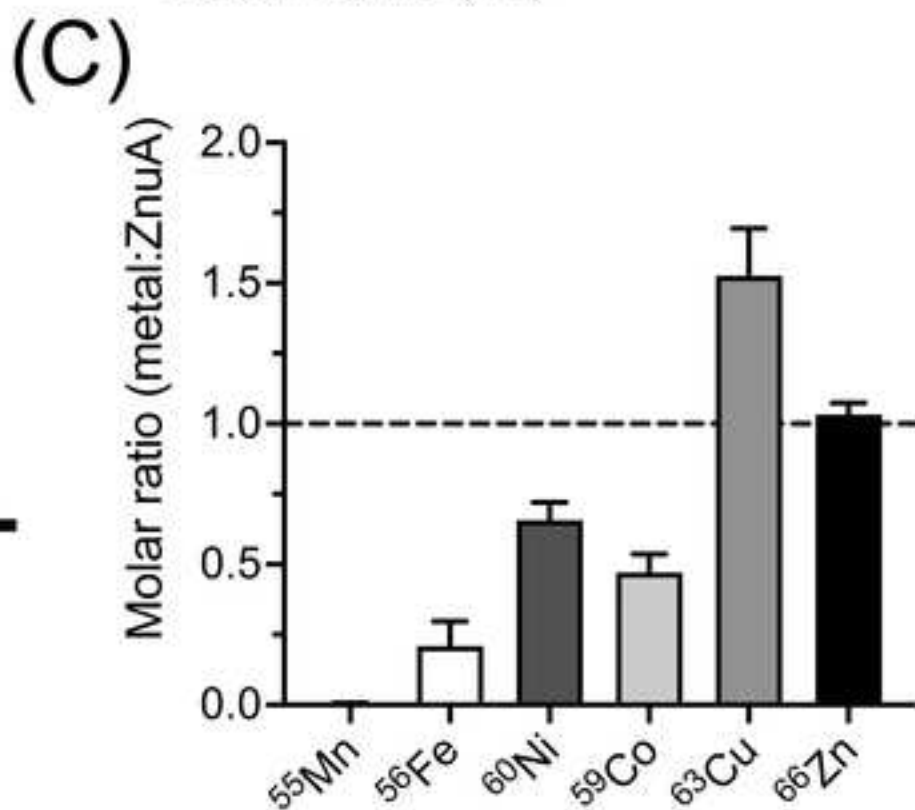
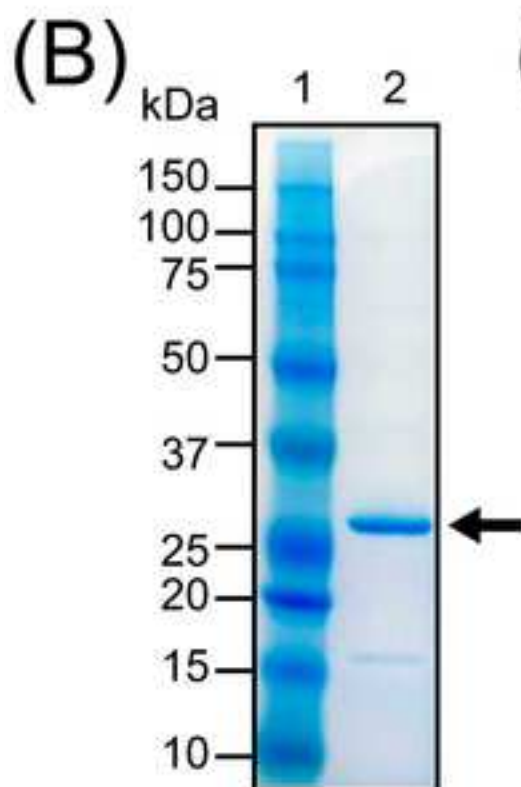
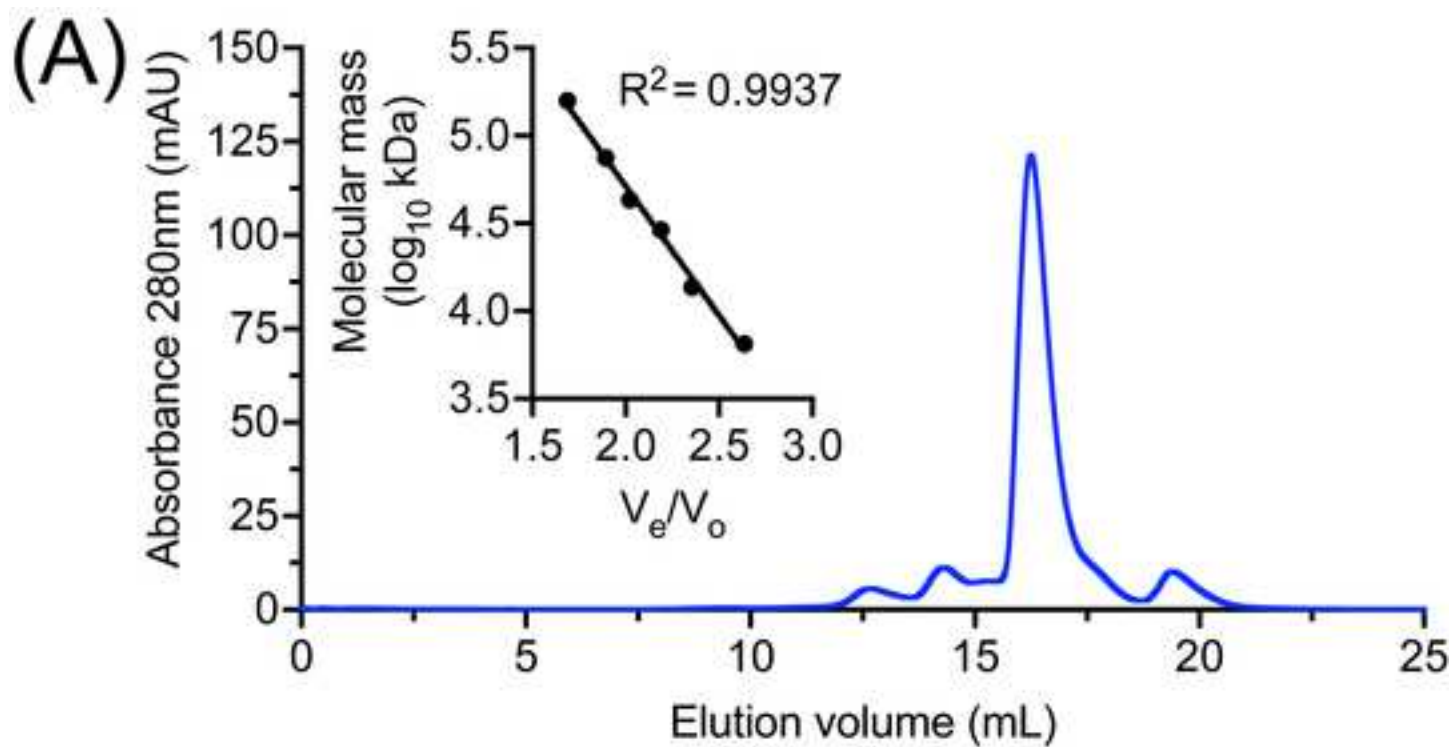
$T_m$ , melting transition

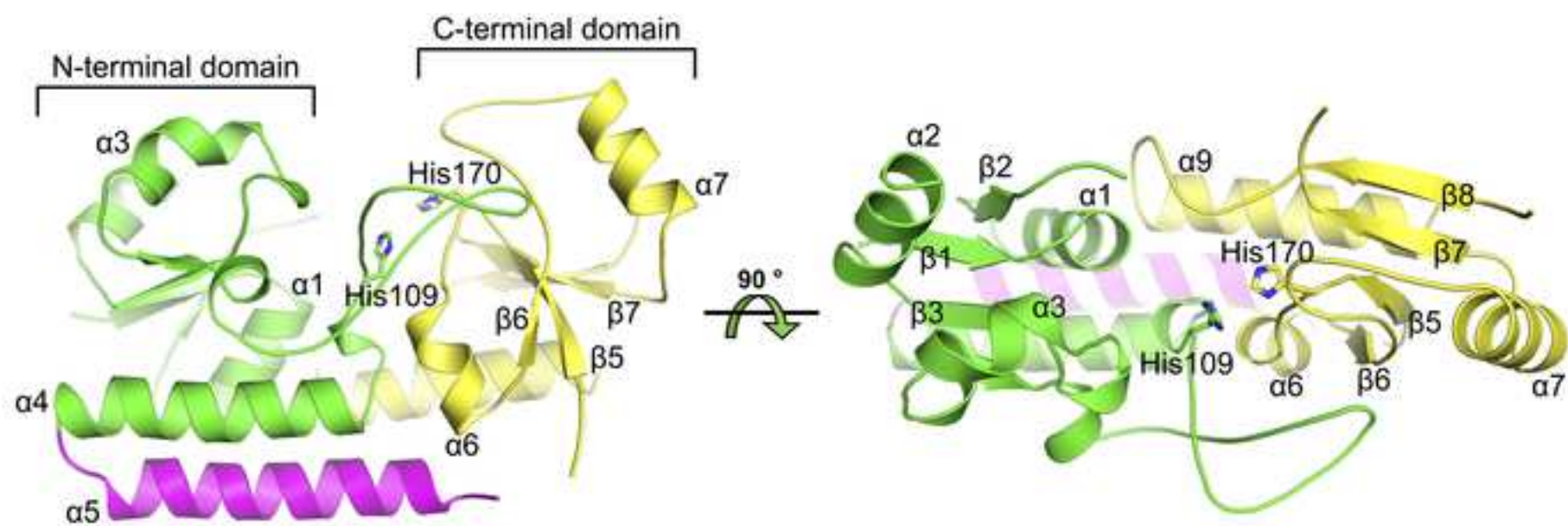
WHO, World Health Organization

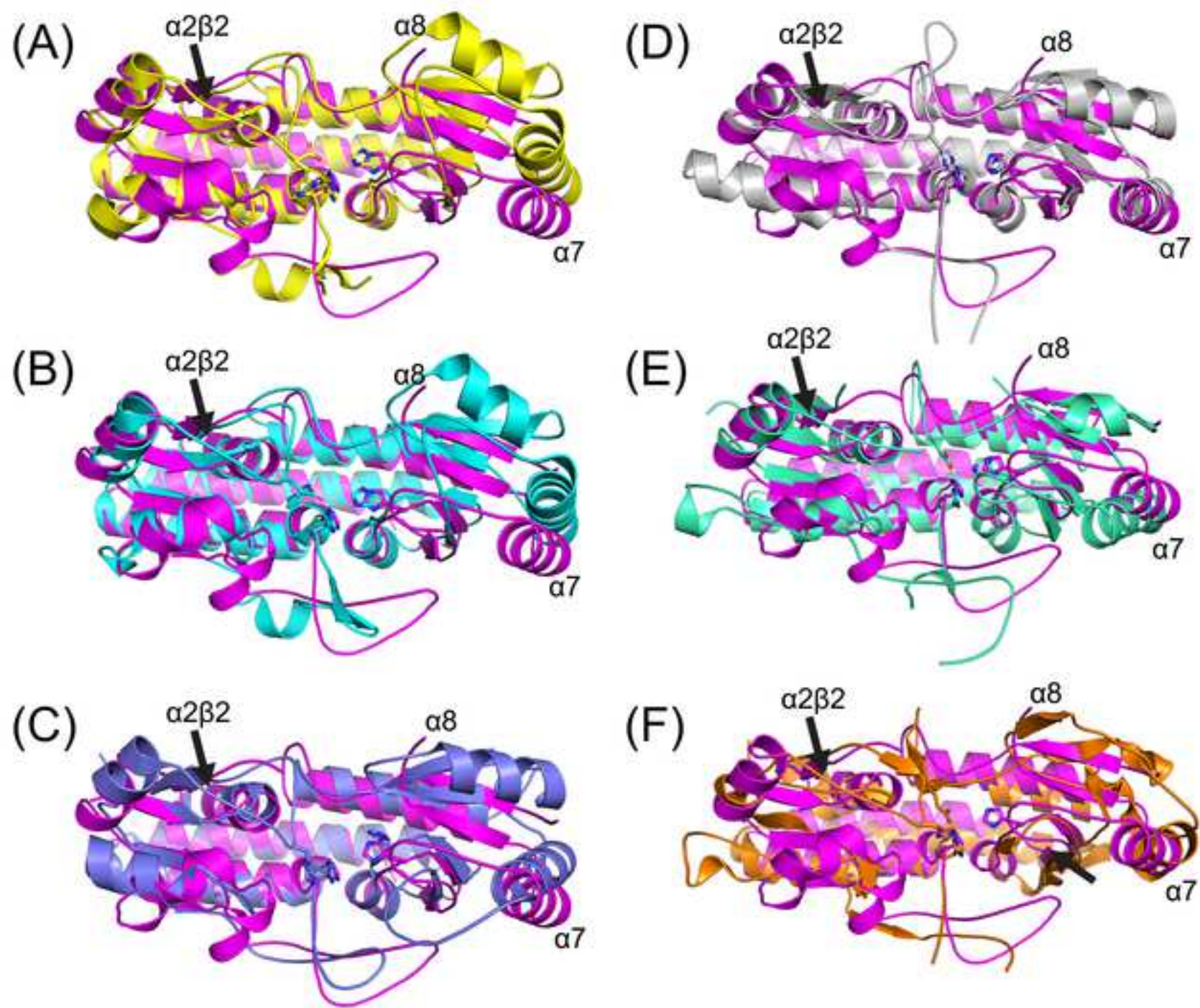
(A) Sequence percentage identity to *A. baumannii* ZnuA

## (B)

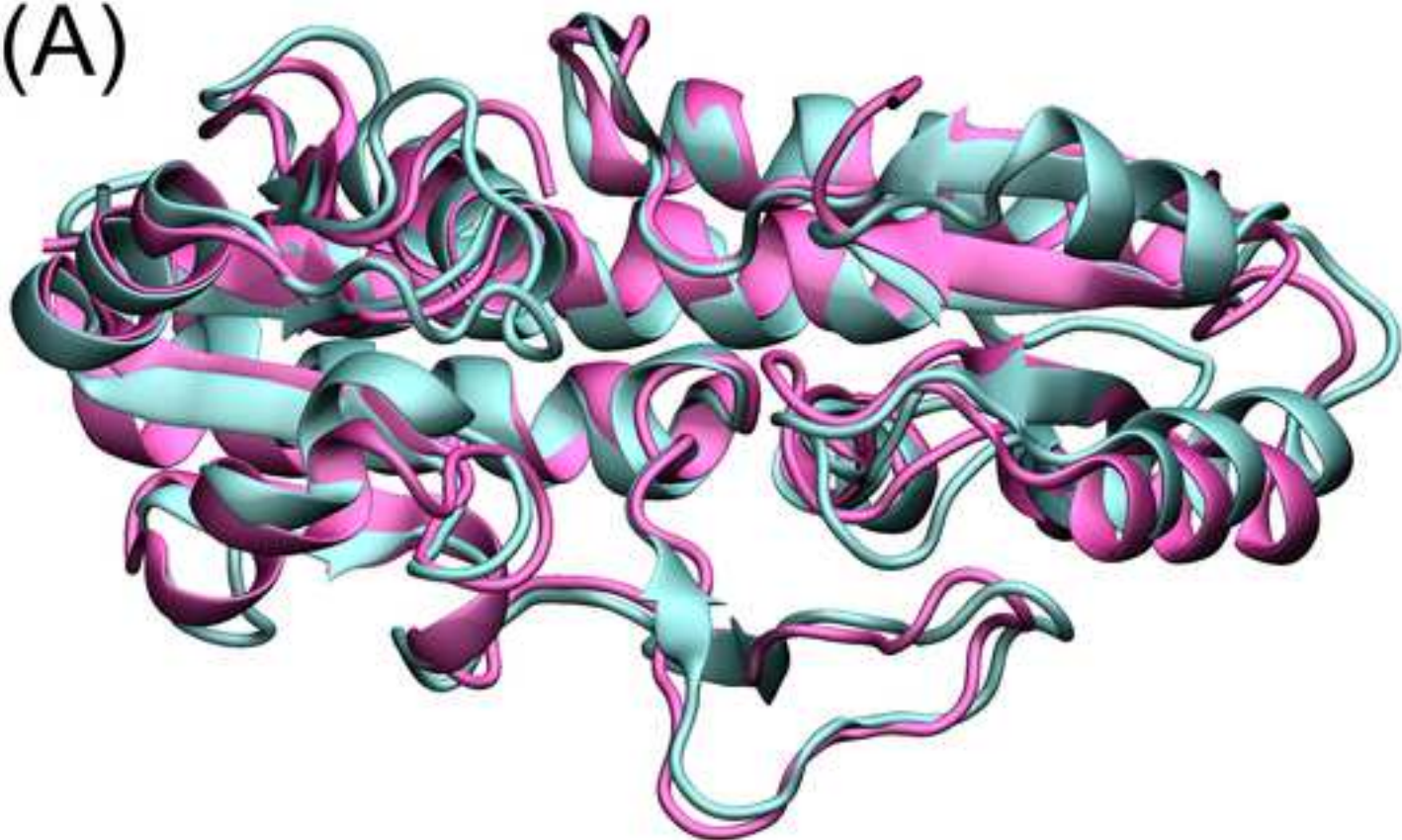
Ab_ZnuA	-----MSTLGSQGLVSTHPIYLIAKEITKGV EEPQLLL-QGQS	39
Pau_ZnuA	MTLRPFALLSTC--FALFLASPARAEVSVLTSIKPLQLVAAAIQDGVGQPDVLLPPGAS	58
Vpa_ZnuA	MLSR YFL-----LTVAALFA--QSASAIEVLTSIKPIQMITYELMLGTGTPDVLLPSGAS	53
Ype_ZnuA	MLHKNKWLKQAMLASALLLANPFNLASA AVVTSIRPLGFIAAAIADGVLPT EVLLPDGAS	60
Eco_ZnuA	MLHKKTLLFAAL--SAALWGGATQAADA AVVASLKPVGFIASAIADGVTETEVLLPDGAS	58
Sen_ZnuA	MLQKNTLLFAAL--SAALWGSATQAADA AVVASLKPGLGFIA SAIADGVTDTQVLLPDGAS	58
Ab_ZnuA	GH DVQLTPAHRKAIN DATLVIWLGKAHEAPLNKLLSNNKKAIALLD SGILSILP---Q--	94
Pau_ZnuA	PHQYALRPSDVRRLE REVQLFYWIGPDLENFLPKVLAGRQGTS-VAVQDLPGMH---LR-K	113
Vpa_ZnuA	PHDYALRPSDVKRIQQADLVIWVFGQDLEFPMSKLEGRTS--AL TLSQVFNLA---L-RE	107
Ype_ZnuA	PHDYALRPSDVQRLRS AELVIWVGP EMEAFLSKPLTQVAENKQIALS QLP SVTPLL MKSD	120
Eco_ZnuA	EH DYSLRPSDVKRLQ NADLVVWVGP EMEAFM QKPVSKLPGAKQVTIA QLEDVKP LLMKSI	118
Sen_ZnuA	EH DYSLRPSDVKRLQ GADLVVWVGP EMEAFMEKSVRNIPDNKQVTIA QLADVKP LLMKGA	118
Ab_ZnuA	-----RNRGAALPNTVDTHVWLEPNNAVRIGFFIAALRSQQHPENK	136
Pau_ZnuA	FVNFEEEHAGH-----DEHDHHRPGMLDANLWLLPANARTI AARMAEDLAQVDPANA	167
Vpa_ZnuA	YGE E-----QHEHDGHHHGHYDPHF WLGI GPVGVASAI TAKLIELDADQQ	154
Ype_ZnuA	EHDEAE EGS GHHHDHAKDNPTDDHHHGEYNM IWLSPAI AKQAAIAIHDRLLELTPQNK	180
Eco_ZnuA	HGDDDDPHDHA-----EKSD EDBH HGD FNM L WLSPEIARATAVAIHGKLV E LMPQSR	170
Sen_ZnuA	DDDEDEHANTGA----DEEKGDVHHHHGEYNM L WLSPEIARATAVAIHEKLV E LMPQSR	174
Ab_ZnuA	AKYWNNA NTFARNMLQAAQAY---DSSSNGKPYWSYH DAYQY LERSLNLKFAGAL TDDPH	193
Pau_ZnuA	GRYRANLKA FDERLGGLDGKLRERLGKLAGK PFFVFEAFDYFEEAYGLRHTGVFAVSAE	227
Vpa_ZnuA	QQYQDNLVRFLANLAEQDNTIG EKLKPVTTVPYYVFDAYGYFEQH FALNNLGHFTV SPE	214
Ype_ZnuA	DKLDANLRRFEYQLAQNEKNIVTMLKPVQ GKGYFVFDAYGYFENHFGLSPLGHFTVNPE	240
Eco_ZnuA	AKLDANLKD FEAQLASTETQVGNELAPLKGKGYFVFDAYGYFEKQFGLTPLGHFTVNPE	230
Sen_ZnuA	AKLDANLKD FEAQLAATDKQVGNELAPLKGKGYFVFDAYGYFEKHYGLTPLGHFTVNPE	234
Ab_ZnuA	VAPTAAQIKYL NDSR--PKAQMCLLAESFT-----TKGQYQKLSITFPQVDES MN-	243
Pau_ZnuA	VQPGARHVAAMRAQLKAAGPACIFSE PPLRPR LADTLSEGLPVRLAEL--DDLGVNVSV D	285
Vpa_ZnuA	RKPGAKTLIAIKKTLNDQLAKCVFSE PQFEPAI IETVVRGTSAKIGVL--DPLGISIELQ	272
Ype_ZnuA	IQPGAQR LHQIRTQLVEHKAVCVFAEPQFRPAVINAVAKGTNVRSGTL--DPLGSGIVLD	298
Eco_ZnuA	IQPGAQR LH EIRTQLVEQKATCVFAEPQFRPAVVE SVARGTSVRMGTL--DPLGTNIKLG	288
Sen_ZnuA	IQPGAQR LH EIRTQLVEQKATCVFAEPQFRPAVVEAVARGTSVRMGTL--DPLGTNIKLG	292
Ab_ZnuA	EDNFVTA WKKLAIKTDKCVLNTQK	267
Pau_ZnuA	ANGYENLLNNLAGEFAGCLEKL--	307
Vpa_ZnuA	AGSYFAPLNSLAESYYACL SQS--	294
Ype_ZnuA	KDSYVNFLSQLSNQYV SCLK----	318
Eco_ZnuA	KTSYSEFLSQLANQYASCLKGD--	310
Sen_ZnuA	KTSYSAFLSQLANQYASCLKGD--	314



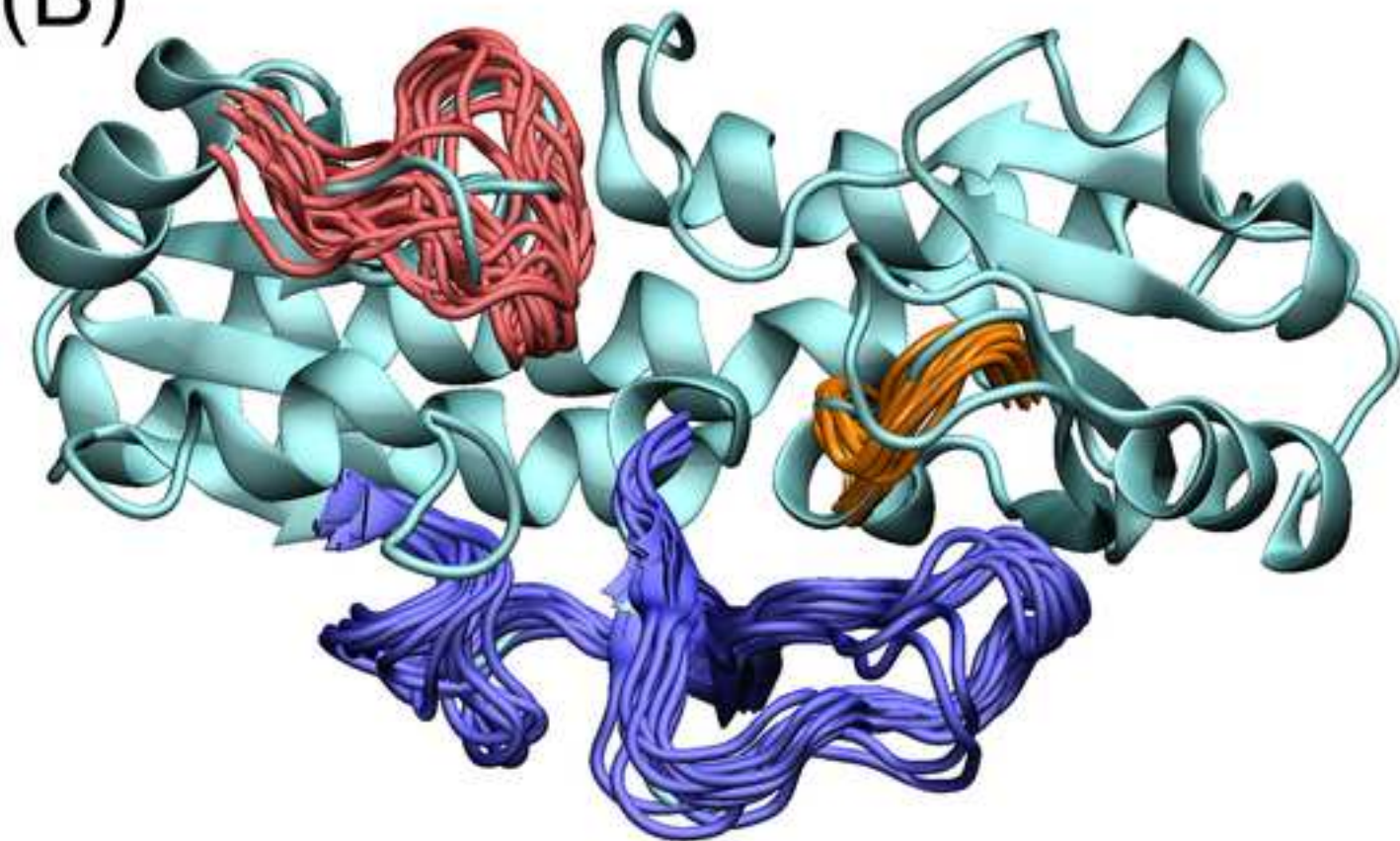


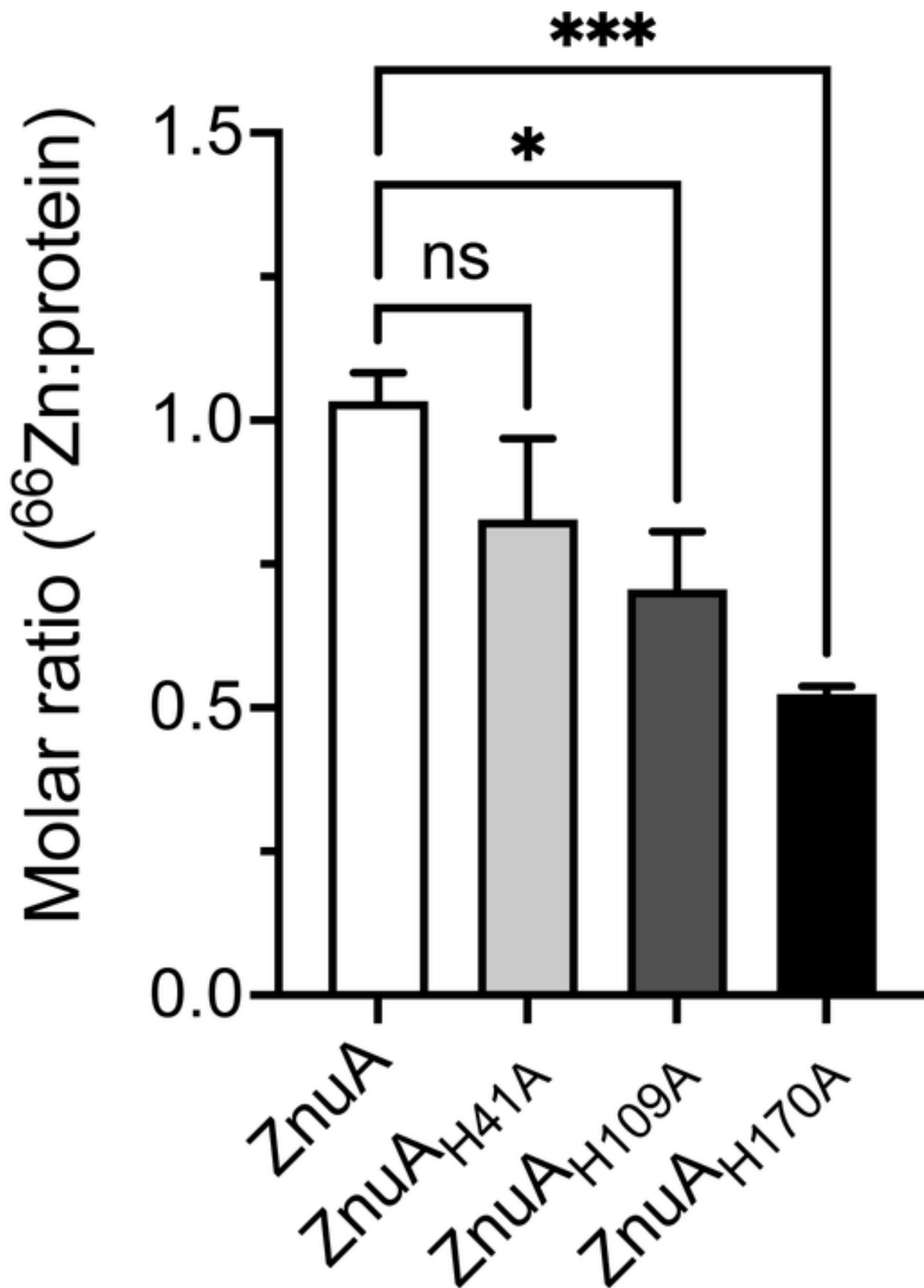


(A)



(B)





### Declaration of interests

The authors declare that they have no known competing financial interests or personal relationships that could have appeared to influence the work reported in this paper.

The authors declare the following financial interests/personal relationships which may be considered as potential competing interests:

Christopher McDevitt reports financial support was provided by National Health and Medical Research Council. Christopher McDevitt reports financial support was provided by Australian Research Council. Bostjan Kobe reports financial support was provided by National Health and Medical Research Council. Bostjan Kobe reports financial support was provided by Australian Research Council.

Saleh Alquethamy: Investigation, Methodology, Data curation, Formal analysis, Writing-Original draft preparation.

Katherine Ganio: Investigation.

Zhenyao Luo: Investigation, Formal analysis, Visualization.

Sheik Imammul Hossain: Investigation, Formal analysis, Visualization.

Andrew J. Hayes: Investigation, Formal analysis.

Thomas Ve: Formal analysis.

Mark R. Davies: Formal analysis, Supervision.

Evelyne Deplazes: Investigation, Formal analysis, Funding acquisition, Writing - Review & Editing.

Boštjan Kobe: Writing - Review & Editing, Supervision, Funding acquisition.

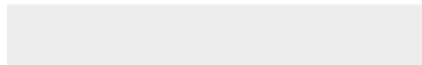
Christopher A. McDevitt: Conceptualization, Methodology, Resources, Formal analysis, Writing - Original Draft, Writing - Review & Editing, Supervision, Project administration, Funding acquisition.




Click here to access/download

**Supplementary Material**

Alquethamy\_Supplementary\_Final.pdf





Click here to access/download  
**Supplementary Material**  
Table S3.xlsx